Science

AAAS

Supplementary Materials for

Ablation of CaMKIIδ oxidation by CRISPR-Cas9 base editing as a therapy for cardiac disease

Simon Lebek *et al*.

Corresponding author: Eric N. Olson, eric.olson@utsouthwestern.edu

The PDF file includes:

Other Supplementary Material for this manuscript includes the following:

Materials and Methods

Study design and approval

The aim of the present study was to develop a therapeutic approach for cardiac disease by using CRISPR-Cas9 nucleotide base editing. We designed a gene editing system to ablate the oxidative activation sites of CaMKIIδ, which cause pathological enzyme activation. Different editing approaches were first screened in HEK293 cells. The two most efficient sgRNAs were then tested for their biologic effect in human cardiomyocytes derived from induced pluripotent stem cells (iPSCs). We then applied the CRISPR-Cas9 base editing system with the best therapeutic in vitro effect to adult mice that were subjected to ischemia/reperfusion (IR) injury.

All experiments were performed in replicates. For all in vivo experiments, we used eight C57Bl6 mice at 12 weeks of age per group. Mice were randomly assigned to sham surgery or to IR with either no injection, intracardiac injection of a control virus or intracardiac injection of a *CaMKIIδ* editing system. Echocardiography was performed on each mouse before IR as well as 24 hours, one week, two weeks, and three weeks after IR. Cardiac magnetic resonance imaging was performed in five mice per group at four weeks post-IR. After five weeks, all mice were euthanized, and five out of eight mice per group were dedicated to molecular analyses and three mice to histological analyses. We did not use a statistical test to predetermine the sample size. All samples are included in the study, with no data excluded. Each experimental procedure involving animals has been reviewed and approved by the University of Texas Southwestern Medical Center's Institutional Animal Care and Use Committee.

Plasmids and cloning

Plasmids were ordered from Addgene. The sgRNAs (listed in table S1) were cloned into a pmCherry_gRNA plasmid containing a U6-driven sgRNA scaffold and a cytomegalovirus (CMV)–driven pmCherry fluorescent protein (gift from Ervin Welker, Addgene plasmid #80457, http://n2t.net/addgene:80457; RRID: Addgene_80457).

pCMV_ABEmax_P2A_GFP (Addgene plasmid #112101, http://n2t.net/addgene:112101, RRID: Addgene_112101) (*23*), NG-ABEmax (Addgene plasmid #124163, http://n2t.net/addgene:124163, RRID: Addgene_124163) (*33*), ABE8e (Addgene plasmid #138489, http://n2t.net/addgene:138489, RRID: Addgene_138489) (*3*), and NG-ABE8e (Addgene #138491, http://n2t.net/addgene:138491, RRID: Addgene_138491) (*3*) were gifts from David Liu. pCMV-T7-ABEmax(7.10)-SpRY-P2A-EGFP (RTW5025) was a gift from Benjamin Kleinstiver (Addgene plasmid #140003, http://n2t.net/addgene:140003, RRID: Addgene_140003) (*24*). ABE8e-SpRY was obtained by adapting pCMV-T7-ABEmax(7.10)-SpRY-P2A-EGFP (RTW5025).

For the in vivo experiments, the N- and C-terminal ABE constructs were adapted from Cbh_v5 AAV-ABE N-terminal (gift from David Liu, Addgene plasmid #137177, http://n2t.net/addgene:137177, RRID: Addgene_137177) (*34*) and Cbh_v5 AAV-ABE C-terminal (gift from David Liu, Addgene plasmid #137178, http://n2t.net/addgene:137178, RRID: Addgene_137178) (*34*), respectively, to carry ABE8e-SpRY (driven by a cardiac troponin T promoter) and mouse sgRNA6 (driven by a U6 promoter). A split-intein trans-splicing system enabled reassembly to a functional ABE system in vivo, as previously described (*2*).

Adaptions were performed using oligonucleotides (IDT) or products of PCR amplification of appropriate template sequences with PrimeStar GXL Polymerase (Takara). Oligonucleotides and PCR products were cloned into restriction enzyme-digested vectors using NEBuilder HiFi DNA Assembly (NEB).

TOPO-TA (topoisomerase-based thymine adenine) cloning of cDNA PCR products (TOPO™ TA Cloning™ Kit, Invitrogen) with subsequent sequencing was used to further confirm successful gene editing in vivo.

Cell culture and transfection

HEK293 (ATCC) and N2a (ATCC) cells were cultured in Dulbecco's modified Eagle's medium (Sigma-Aldrich) containing 10% (v/v) fetal bovine serum (GeminiBio). For transfection, cells were plated onto 24-well plates (Corning) with approximately 125,000 cells per well. After 24 h, cells were transfected with plasmids expressing the base editing components using Lipofectamine 2000 (Thermo Fisher Scientific) according to the manufacturer's instructions. Three days after the transfection, cells were harvested to assess the editing efficiency.

Human iPSC culture and nucleofection

Human iPSCs (previously generated and used in our laboratory (2)) were maintained on Matrigel (Corning)-coated 6-well polystyrene culture plates in mTeSR™1 media (STEMCELL). At 70-80% confluency, they were passaged using Versene (Thermo Fisher Scientific).

Approximately 8×10^5 iPSCs were used for nucleofection experiments and they were subjected to 10 µM ROCK inhibitor (Y-27632, Selleckchem) one hour earlier. Single cell status was obtained using Accutase (Innovative Cell Technologies). The iPSCs were mixed either with 1.5 µg of pmCherry_gRNA plasmid carrying sgRNA1 and 4.5 µg ABE8e plasmid or with 1.5 µg of pmCherry_gRNA plasmid carrying sgRNA6 and 4.5 µg ABE8e-SpRY plasmid. P3 Primary Cell 4D-Nucleofector X Kit (Lonza) was used according to the manufacturer's protocol to nucleofect iPSCs. ROCK inhibitor (10 µM) and Primocin (100 µg/mL) (InvivoGen) were then added to the culture media and incubated for one day. Two days after the nucleofection, pmCherry and green fluorescent protein (GFP) double-positive cells were collected by fluorescence-activated cell sorting and clonally expanded to establish the M281V (sgRNA1) and MMH281/282/283VVR (sgRNA6) iPSC lines.

Sanger sequencing analysis

DirectPCR cell lysis reagent (Viagen) with proteinase K (1 µg/µL) was used according to the manufacturer's recommendations to isolate genomic DNA of human HEK293 cells, human iPSCs, and mouse N2a cells. DNA was amplified using PrimeSTAR GXL DNA polymerase (Takara) with the primers listed in table S2 and the PCR product was cleaned using ExoSap-IT Express (Thermo Fisher Scientific). The editing efficiency was determined by analyzing the Sanger chromatograms with EditR (*35*).

Deep amplicon sequencing analysis

Deep amplicon sequencing was used to measure the on-target editing efficiency for *CaMKIIδ* in human iPSCs and in cardiac tissue from mice treated with AAV-ABE-sgRNA6. DNeasy Blood & Tissue Kit (Qiagen) was used to isolate genomic DNA. TRIzol (Thermo Fisher Scientific) and RNeasy Mini Kit (Qiagen) were used to isolate total RNA from whole hearts that was reverse transcribed using iScript Reverse Transcription Supermix (Bio-Rad) with random primers. On-target sites for human *CaMKIIδ* DNA, mouse *CaMKIIδ* DNA, and mouse CaMKIIδ cDNA were PCR amplified using PrimeStar GXL Polymerase (Takara) with the primers listed in table S3. In a second PCR round, Illumina flow cell binding sequences and barcodes were added. AMPure XP Beads (Beckman Coulter) were used to purify PCR products that were then tested for integrity on a 2200 TapeStation System (Agilent). After quantification of DNA concentration by QuBit dsDNA high-sensitivity assay (Invitrogen), samples were pooled and loaded onto an Illumina MiSeq. After demultiplexing, amplicon reads were analyzed for editing efficiency using CRISPResso2 (*26*).

Off-target analyses

Deep amplicon sequencing (described above) was used to measure several important genes for potential off-target editing of ABE8e-SpRY and sgRNA6. First, potential editing of other *CaMKII* isoforms (*α*, *β*, and *γ*) was measured in human iPSCs after nucleofection of ABE components using the primers listed in table S3. Using the cutting frequency determination (CFD) score of CRISPOR, we identified the next top eight candidate off-target sites in the human genome (table S4) and evaluated them in human iPSCs with the primers listed in table S5 (*25*).

Besides *CaMKIIδ*, we also measured potential editing of other *CaMKII* isoforms (*α*, *β*, and *γ*) in mouse hearts injected with AAV-ABE-sgRNA6. Since targeting CaMKII in organs other than heart may have potentially severe adverse side effects, we tested for off-organ editing in the brain, which expresses all *CaMKII* isoforms, the tibialis anterior muscle (for *CaMKIIδ*), and the liver (for *CaMKIIδ*). Editing of *CaMKIIδ* was also analyzed in mice that were injected with a control virus encoding either half of the split adenine base editor (double N- or C-term AAV9) to test whether this was a true control and did not edit *CaMKIIδ*.

We reported the formal adenine to guanine editing for each adenine along the DNA sequences corresponding to sgRNA6. An allele frequency of 0.2% has previously been used as a cut-off to distinguish from unspecific background guanine signal (*26*). This cut-off is displayed in the graphs and adenines with a guanine level below this threshold are considered as not edited.

Quantitative real-time PCR analysis

TRIzol (Thermo Fisher Scientific) and RNeasy Mini Kit (Qiagen) were used to isolate total RNA. Following reverse transcription with iScript Reverse Transcription Supermix (Bio-Rad), quantitative polymerase chain reaction (qPCR) was performed using KAPA PROBE FAST qPCR Kit - ROX Low (Roche). TaqMan Gene Expression Assays (all from Thermo Fisher Scientific) for CaMKIIβ (assay ID Hs00365799_m1), CaMKIIδ (assay ID Hs00943547_m1), and GAPDH (assay ID Hs99999905_m1) were performed using a QuantStudio™ 5 Real-Time PCR System (Applied Biosystems). Expression of CaMKIIβ and CaMKIIδ are reported as percentage of GAPDH.

Differentiation of human iPSC into cardiomyocytes

At 70-80% confluency, iPSCs were differentiated into cardiomyocytes by subjecting them to CHIR99021 (Selleckchem) in RPMI supplemented with ascorbic acid (50 µg/mL) and B27 without insulin (RPMI/B27-) for 24 hours (day 0). After that, medium was replaced with RPMI/B27- for 2 days, before replacing it again with RPMI/B27- supplemented with WNT-C59 (Selleckchem). After another 2 days, medium was refreshed with RPMI/B27-. From day 7 onwards, iPSC-cardiomyocytes were cultured in RPMI with ascorbic acid (50 µg/mL) and B27 (RPMI/B27). Beginning on day 10, cells were maintained in RPMI without glucose and supplemented with 5 mM sodium DL-lactate and CDM3 supplement to metabolically select for cardiomyocytes. After 5 days, medium was replaced with RPMI/B27 and refreshed every 3 days. CMs were analyzed after day 30. For all experiments involving iPSC-derived cardiomyocytes, data were collected from at least three independent differentiations.

Simulated ischemia/reperfusion in vitro

Simulated ischemia/reperfusion (IR) with a hypoxia chamber was used to challenge human iPSC-derived cardiomyocytes in vitro, as previously described (36). Regular cardiomyocyte culture medium (RPMI/B27) was replaced by freshly made ischemia Esumi buffer (117 mM NaCl, 12 mM KCl, 0.9 mM $CaCl_2$, 0.49 mM $MgCl_2$, 4 mM HEPES, 20 mM sodium lactate, and 5.6 mM 2-deoxyglucose at pH 6.2) and cardiomyocytes were placed in a MIC-101 Modular Incubator Chamber at 37° C (Billups-Rothenberg). Cardiomyocytes were subjected to simulated ischemia (95% N_2 and 5% CO_2) for five hours. Meanwhile, control cardiomyocytes were exposed to normoxia control medium (137 mM NaCl, 3.8 mM KCl, 0.9 mM $CaCl_2$, 0.49 mM $MgCl_2$, 4 mM

HEPES, and 5.6 mM D-glucose at pH 7.4). After five hours, ischemia and normoxia buffers were replaced with fresh culture medium (RPMI/B27). Cells were placed in a regular cell culture incubator for 14 hours reperfusion and were then analyzed.

Western blot analysis

Western blot analysis was performed using either iPSC-derived cardiomyocytes or snap-frozen hearts that were pulverized with a tissue crusher. Proteins were isolated using RIPA buffer (Sigma-Aldrich) supplemented with protease- and phosphatase-inhibitors (Roche). Sonication with a Bioruptor Pico (Diagenode, 10 cycles of 30 s sonication on and 30 s off) was used to break genomic DNA. Samples were then centrifuged for 15 min at 10,000 x g at 4º C and supernatant was stored at -80º C. Protein concentration was measured with a BCA assay (Thermo Fisher Scientific) and equal amounts of protein were loaded on a Mini-PROTEAN® TGX™ gel (Bio-Rad). Proteins were transferred on a polyvinylidene fluoride membrane (Millipore), blocked in 5% milk in TBS-Tween 0.1% and incubated at 4º C overnight with the primary antibody: rabbit polyclonal anti-oxCaMKII (1:1,000, Sigma-Aldrich, catalog number 07-1387), rabbit polyclonal anti-pCaMKII (1:1,000, Invitrogen, catalog number PA5-37833), mouse monoclonal anti-CaMKII (1:1,000, BD Biosciences, catalog number 611293), rabbit polyclonal anti-pRyR2 (at serine 2814, 1:1,000, Badrilla, catalog number A010-31AP), rabbit polyclonal anti-RyR2 (1:1,000, Sigma-Aldrich, catalog number HPA020028), and mouse monoclonal anti-GAPDH (1:1,000, Sigma-Aldrich, catalog number MAB374). Secondary antibodies were HRP-conjugated goat anti-rabbit (1:10,000, Bio-Rad, catalog number 1706515) and HRP-conjugated goat anti-mouse (1:10,000, Bio-Rad, catalog number 1706516) and were incubated for one hour at room temperature.

Immunodetection was done on a ChemiDoc MP Imaging System (Bio-Rad) using Western Blotting Luminol Reagent (Santa Cruz Biotechnology). Mean densitometric analysis was performed using ImageJ.

Measurement of CaMKII activity

CaMKII activity assays were performed with iPSC-derived cardiomyocytes and with snap-frozen hearts that were pulverized with a tissue crusher. Proteins were isolated in 1% (v/v) Triton X-100, 20 mM Tris, 100 mM NaCl supplemented with protease- and phosphatase-inhibitors (Roche) at a pH of 7.4. After centrifugation for 15 min at 10,000 x g at 4º C, the supernatant was collected. Equal volumes were loaded to the CycLex® CaM-kinase II assay kit (MBL International Corporation) that was performed according to the manufacturer's recommendations and absorbance at 450 nm was measured with a CLARIOstar microplate reader (BMG LABTECH). Some experiments were performed in presence of 1 μM of the CaMKII inhibitor myristoylated autocamtide-2 related inhibitory peptide (AIP, Sigma-Aldrich, diluted in Kinase Buffer of the CycLex® CaM-kinase II assay kit). A standard curve was generated using the CaM-kinase II Positive Control (MBL International Corporation). The measured CaMKII activity of each sample was then normalized to the protein concentration of the lysate (BCA assay, Thermo Fisher Scientific).

Measurements of cellular Ca^{2+} characteristics

Cellular Ca^{2+} characteristics were assessed using epifluorescence microscopy. Human iPSC-derived cardiomyocytes were replated on a glass bottom microwell dish (MatTek Corporation) to a single cell density and were cultured for one week in RPMI/B27 to acclimate and reach a steady-state status. On the day of the experiment, cardiomyocytes were loaded with 5 µM Fura-2 AM (20 min at 37º C, Invitrogen) and were mounted on an inverted microscope (Motic AE31E). Ca^{2+} dynamics was measured using a fluorescence detection system (IonOptix) and Fura-2 fluorescence emission ratio was obtained by alternating excitation at 340 nm and 380 nm (switching rate 1,000 Hz).

Before the measurement was started, cardiomyocytes were incubated for 15 min with Tyrode's solution (140 mmol/l NaCl, 4 mmol/l KCl, 1 mmol/l $MgCl_2$, 10 mmol/l HEPES, 10 mmol/l Glucose, 1.25 mmol/l $CaCl_2$, pH=7.4) to ensure de-esterification of intracellular Fura-2 AM. Regular Ca^{2+} transients were measured at a steady-state status under electrical field stimulation (1 Hz with a 5 ms pulse of 30 V). Ca^{2+} transient characteristics and the occurrence of arrhythmias were analyzed using IonWizard 6.0 analysis software (IonOptix).

Ischemia/reperfusion injury in adult mice

Male C57Bl6 wildtype mice (Charles River) were housed in a standard mouse facility with a regular 12-hour light/dark cycle and received standard chow (2916 Teklad Global). At 12 weeks of age, ischemia/reperfusion (IR) surgery was performed in mice anesthetized with Ketamine/Xylazine complex, intubated, and ventilated with a MiniVent mouse ventilator (Hugo Sachs Elektronik, 105 breaths per minute, 250 µL stroke volume). Using a rectal probe, mouse

body temperature was monitored and kept close to 37.0° C. All surgeries were performed by the same experienced surgeon in a standardized manner. Thoracotomy was performed between the left fourth and fifth ribs, a 7-0 nylon suture was set under the left anterior descending coronary artery, and a non-traumatic occluder was put on the artery for 45 min of ischemia. The ligature was then released and the CRISPR-Cas9 components were injected straight to the heart into the area of injury. While eight mice were injected with a functional (N- and C-term) CRISPR-Cas9 editing system (IR+Edit), another eight mice received a non-functional control virus injection, containing either the double amount of the C- or N-term of the AAV9 (IR+Control Virus). All mice were injected with $7.5x10^{11}$ vg/kg bodyweight of each N- and C-term AAV9, resulting in a total virus amount of $1.5x10^{12}$ vg/kg bodyweight. The intracardiac injections (single bolus of 30 µL volume) were performed by the mouse surgeon, who was blinded to the content of liquid. Eight more mice were subjected to IR injury without any injection and another eight mice were subjected to 45 min open chest without IR and without injection (sham). After that, the chest was carefully closed in layers and the mice were allowed to recover.

Virus production

Adeno-associated virus serotype-9 (AAV9) was produced by the Boston Children's Hospital Viral Core. Using discontinuous iodixanol gradients (Cosmo Bio, AXS-1114542-5) AAV9 vectors were purified and then concentrated with a Millipore Amicon filter unit (UFC910008, 100 kDa). Quantitative real-time PCR assays were used to measure AAV9 titers.

Transsthoracic echocardiography

Cardiac function was assessed in conscious mice using two-dimensional transthoracic echocardiography (VisualSonics Vevo2100 imaging system). M-mode traces were acquired, and analysis is based on the average of three consecutive heart beats. Left ventricular end-diastolic (LVIDd) and end-systolic (LVIDs) internal diameter were measured in M-mode tracings. Fractional shortening (%) was calculated by [(LVIDd – LVIDs) / LVIDd] × 100. Heart rate was calculated based on the interval of three consecutive heart beats. Echocardiography was performed one week before the IR injury as well as 24 hours, one week, two weeks, and three weeks after the IR. Each echocardiography was performed and analyzed by the same experienced operator blinded to the study.

Magnetic resonance imaging

Cardiac magnetic resonance imaging (MRI) was performed in mice by the University of Texas Southwestern Medical Center's Advanced Imaging Research Center on a 7-tesla pre-clinical scanner (Bruker Biospec, Germany) using a 72 mm volume transmitter coil with a 2x2 phased array surface receiver coil. Mice were anesthetized by inhalation of 1.5–2.5% isoflurane. The animal's ambient temperature was maintained at 28° C using a Small Rodent Air Heater System (SA Instruments, Stony Brook, NY). A self-gated gradient echo (IntraGate, Bruker Biospin) sequence was used to obtain cine images in the short axis plane. The following imaging parameters were used: TE/TR=3.9/10 ms; number of k-space lines per R-R=1; slice thickness=1 mm, number of averages=3; flip=15°; FOV=30×30 mm^2; matrix=192×192; in-plane resolution=0.15×0.15 mm^3. Five to six contiguous slices were acquired. Segment version 3.0 (http://segment.heiberg.se)

was used to analyze cardiac cine images and left ventricular volumes as well as ejection fraction were calculated (*37*). Each MRI was performed and analyzed by the same experienced operator blinded to the study.

RNA sequencing

Snap-frozen cardiac mouse samples were homogenized in TRIzol (Thermo Fisher Scientific) using a Precellys Evolution homogenizer (Bertin Instruments, 3 cycles x 20 s at 6,800 rpm). RNeasy Micro Kit (Qiagen) was used to isolate RNA, according to manufacturer's recommendations. KAPA mRNA HyperPrep kit (Kapa Biosystems) was used according to the manufacturer's instructions to prepare the RNA sequencing libraries. Using an Illumina NextSeq500 sequencer, high output 75 cycles single-ended sequencing was performed by the University of Texas Southwestern Medical Center CRI Sequencing Facility.

Analysis of RNA sequencing data

The FastQC tool (version 0.11.8) was used for quality control to determine low quality and adaptor portion of the reads for trimming. Trimmomatic (version 0.39) was used for read-trimming and trimmed reads were aligned to the mouse reference genome (mm10) using HiSAT2 (version 2.1.0, default settings). Count matrix for each sample was produced by counting aligned reads using featureCounts (version 1.6.2) and raw count matrix was used for differential gene expression analysis using DESeq package (version 1.38.0) in R (version 3.5.1). For the principal component analysis (PCA), the raw counts of all samples were normalized using the rlog function in R. The

normalized values were then used as input for the prcomp function. The calculated PC1 and PC2 scores were visualized in a scatter plot using the ggplot2 package. Analysis of enriched gene sets (gene ontology terms) was performed using Metascape (https://metascape.org/) with the upregulated or downregulated genes as input (*38*).

The average percentage of adenine (A) to inosine (I) editing among adenosines in the transcriptome-wide sequencing analysis was obtained by using a previously described strategy (*6*). The percentage of editing in each sample was quantified using REDItools2. We removed all nucleotides except adenosines and filtered the remaining adenosines with a read coverage of less than 10 or a read quality score below 25 to avoid errors due to a low sampling or sequencing quality. The percentage of the transcriptome-wide A-to-I editing was calculated by dividing the number of A-to-I conversions in each sample by the total number of adenosines in our dataset after filtering.

Histology and Immunohistochemistry

For routine histology, TUNEL, and immunohistochemistry, mouse hearts were dissected out and cleaned in phosphate-buffered saline (PBS) containing cardioplegic 0.2 M KCl for 5 minutes before fixating in 10% neutral-buffered formalin (Sigma-Aldrich) overnight at room temperature. Then, samples were dehydrated in 70% ethanol and embedded in paraffin. Transverse cross-sections 1,500 μm below the expected normoxic myocardium were used for analyses. Sections were mounted on slides and subjected to trichrome and picrosirius red staining and images were captured at 10x magnification on a BZ-X700 microscope (Keyence). The fibrotic tissue was quantified in ImageJ by dividing the collagen positive area by the total area of the cross-section.

Terminal deoxynucleotidyltransferase-mediated UTP end label (TUNEL) staining for apoptotic cells and immunohistochemical staining for troponin I were done on the same section. Sections were deparaffinized in xylene, run to water through graded ethanol, and antigen retrieval was conducted for 20 min heating in 1 mM EDTA (pH 8.0). Sections were further treated with 0.3% Triton X-100 and interceding PBS washes were performed throughout the protocol, before blocking with 3% normal goat serum. Primary antibody was rabbit polyclonal anti-troponin I (1:100, Santa Cruz Biotechnology, catalog number H-170) and was incubated overnight at 4° C. Sections were subsequently incubated with the secondary Cy3-conjugated goat anti-rabbit antibody (1:50, Jackson ImmunoResearch, catalog number 111-165-144) for 30 min at room temperature. To conclude the troponin-I immunohistochemistry, linked antigen, primary, and secondary antibodies in the sections were crosslinked with 4% paraformaldehyde before being subjected to the DeadEnd™ Fluorometric TUNEL System (Promega) according to the manufacturer's recommendations. Sections were further incubated with Hoechst 33342 (1:5,000, Invitrogen, catalog number H3570) for 5 min at room temperature. A LSM 800 confocal microscope (Zeiss) was used to capture images. Apoptotic cells are reported as percentage of the total number of cells.

Treadmill exhaustion test

Exercise performance was evaluated by using the Exer-3/6 rodent treadmill, as previously described (Columbus Instrument) (*28*). To test for potential long-term adverse effects of *CaMKIIδ* editing, we analyzed mice 260 days after intraperitoneal injection of AAV9 (1.5×10^{14} vg/kg bodyweight of each N- and C-term) at P5 as well as non-injected littermates. Before the exhaustion

test, all mice were acclimated to the treadmill by three 10 min sessions with a velocity set to 0, 5, and 10 m/min for the first, second, and third day, respectively. The treadmill was inclined to 10° and the electric shock grid at the rear end was turned on (frequency of 3 Hz, stimulation intensity of 10). For the treadmill exhaustion test, mice were first subjected to a warm-up of 10 m/min for 2 min. We then set the velocity to 15 m/min that was accelerated at a rate of 0.6 m/min per minute until the mouse was exhausted. Exhaustion was defined by continuous standing for 5 s on the shock grid, which was evaluated by the same observer for all experiments. Each mouse was subjected to transthoracic echocardiography immediately after exhaustion.

Statistics

Data are presented as mean ± standard error of the mean (SEM). Normal distribution was tested using Shapiro-Wilk normality test. Unpaired Student's *t* test was used for variables that were normally distributed. For variables that were not normally distributed, the Mann-Whitney test was applied. For the comparison of more than two groups that were normally distributed, one-way ANOVA with Holm-Sidak's post-hoc correction was used. Kruskal-Wallis test with Dunn's post-hoc correction was applied for the comparison of more than two groups that were not normally distributed. Two-way ANOVA with Holm-Sidak's post-hoc correction was used for the comparison of more than two groups and two different factors. Categorial data were analyzed using Fisher's exact test. Statistical tests were performed in GraphPad Prism 9. Two-sided p-values below 0.05 were considered statistically significant (*$p < 0.05$, **$p < 0.01$, ***$p < 0.001$, ****$p < 0.0001$).
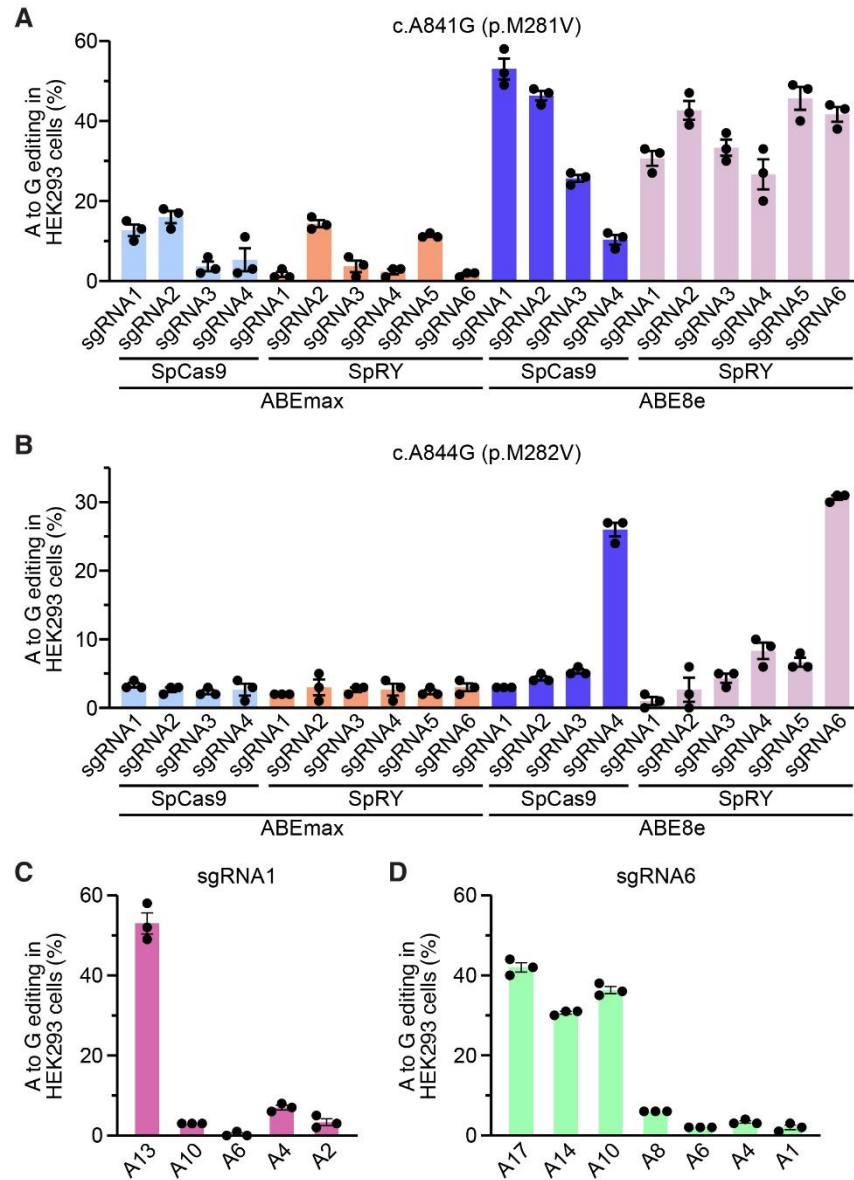
Fig. S1. Screening of various genomic editing strategies of *CaMKIIδ* in HEK293 cells using transfection. (A) Percentage of adenine (A) to guanine (G) editing in human HEK293 cells at c.A841 (p.M281) for sgRNAs 1 to 6 combined with either ABEmax or ABE8e that were fused to either SpCas9 or SpRY. **(B)** Percentage of A to G editing in human HEK293 cells at c.A844 (p.M282) for all tested editing strategies. **(C)** Percentage of A to G editing in HEK293 cells for each adenine in sgRNA1 following base editing with ABE8e fused to SpCas9. **(D)** Percentage of A to G editing in HEK293 cells for each adenine in sgRNA6 following base editing with ABE8e fused to SpRY. Percentage of editing is based on Sanger sequencing. Adenines along the sequence

of either sgRNA1 (C) or sgRNA6 (D) are numbered starting from the PAM. Data are presented as individual data points with means ± SEM.
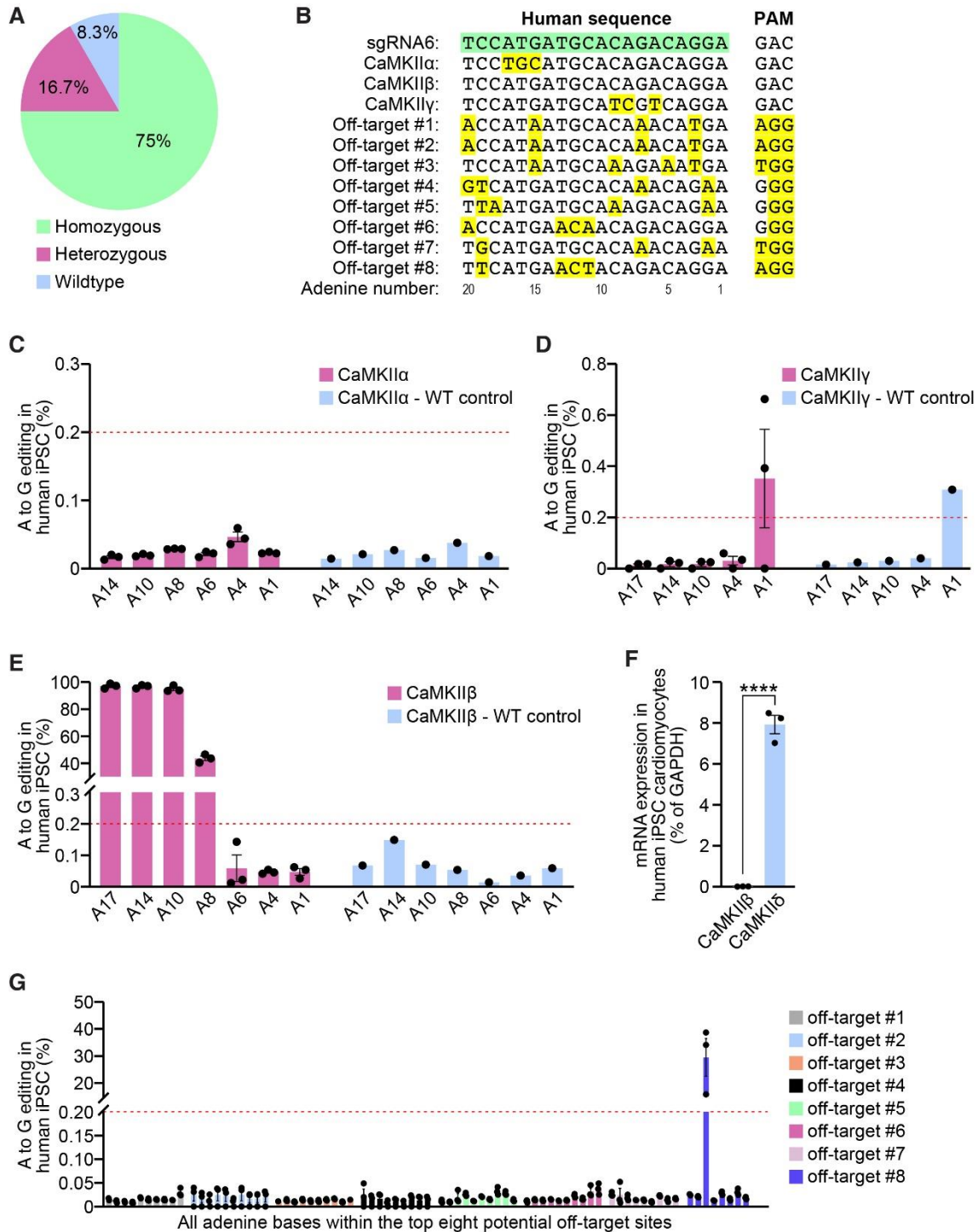
Fig. S2. Analysis of potential genomic off-target editing in human iPSC using deep amplicon sequencing. (A) Percentage of iPSC clones (n=12) that are either wildtype, heterozygous or homozygous for c.A841G (p.M281V), c.A844G (p.M282V), and c.A848G (p.H283R), as determined by Sanger sequencing. **(B)** Sequence of sgRNA6 and the corresponding DNA sequences and PAMs of other *CaMKII* isoforms (*α*, *β*, and *γ*) and of the top eight potential off-target sites predicted by CRISPOR. Bases that are different from sgRNA6 are highlighted in
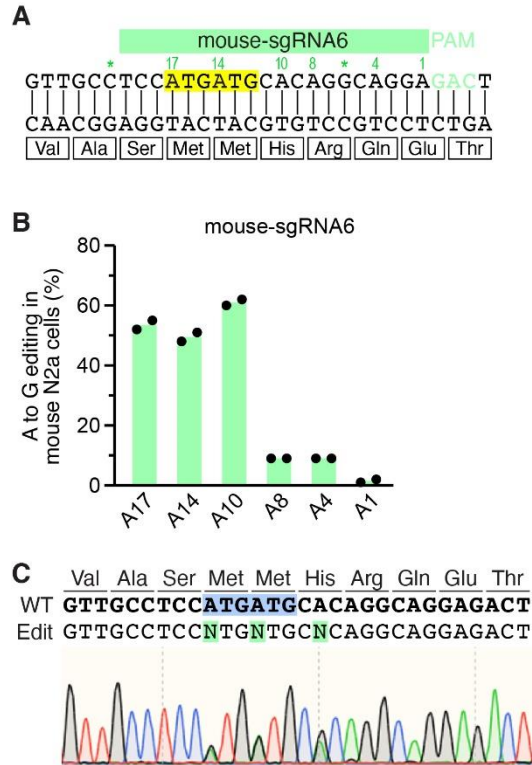
yellow. Adenines along the sequence are numbered starting from the PAM. **(C)** Percentage of adenine (A) to guanine (G) editing for each adenine in the *CaMKIIα* DNA sequence corresponding to sgRNA6. **(D)** Percentage of A to G editing for each adenine in the *CaMKIIγ* DNA sequence corresponding to sgRNA6. **(E)** Percentage of A to G editing for each adenine in the *CaMKIIβ* DNA sequence corresponding to sgRNA6. **(F)** Quantification of CaMKIIβ and CaMKIIδ mRNA expression in human iPSC-CMs. **(G)** Percentage of A to G editing for each adenine (ordered from 5' to 3') in the DNA sequences of the top eight potential off-target sites, starting with #1. Replicates are either human iPSCs (C, D, E, G) from three independent nucleofections with sgRNA6 and ABE8e fused to SpRY, or human cardiomyocytes from three independent differentiations (F). One wildtype iPSC sample was included as a negative control. The red line at 0.2% represents the threshold that has previously been used to distinguish from unspecific background guanine signal (*26*). Statistical comparison is based on an unpaired Student's *t* test (F). Data are presented as individual data points with means ± SEM or as individual data points with means, as appropriate.
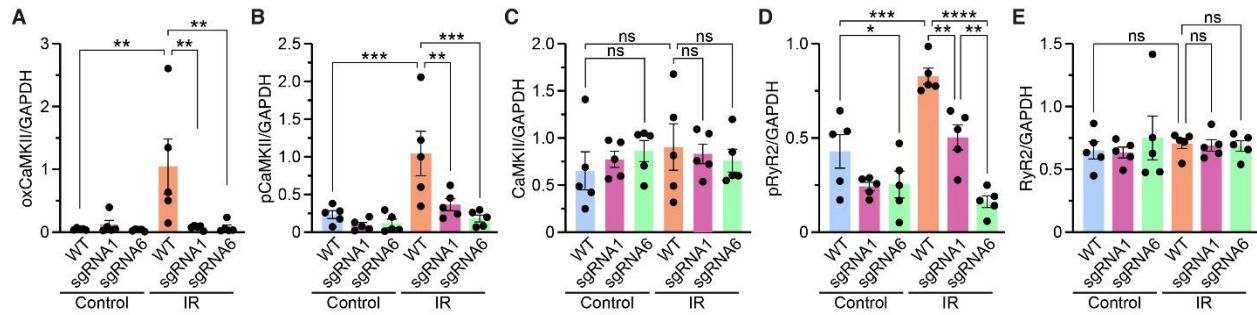
**Fig. S3. Western blot analyses of human iPSC-cardiomyocytes post-IR.** **(A)** Mean densitometric analysis of oxidized CaMKII normalized to GAPDH in human wildtype (WT), sgRNA1, and sgRNA6 iPSC-CMs for control group and following simulated ischemia/reperfusion (IR). **(B)** Mean densitometric analysis for autophosphorylated CaMKII normalized to GAPDH. **(C)** Mean densitometric analysis for total CaMKII normalized to GAPDH. **(D)** Mean densitometric analysis for ryanodine receptor type 2 (RyR2) phosphorylation at the CaMKII site (serine 2814) normalized to GAPDH. **(E)** Mean densitometric analysis for total RyR2 normalized to GAPDH. These data represent further densitometric analyses related to the Western blots presented in the main manuscript. Representative Western blots can be found in Fig. 1E (for A, B, and C) and Fig. 1I (for D and E). Statistical comparisons are based on five independent iPSC-CM differentiations per group and were performed with one-way ANOVA post-hoc corrected by Holm-Sidak. Data are presented as individual data points with means ± SEM.
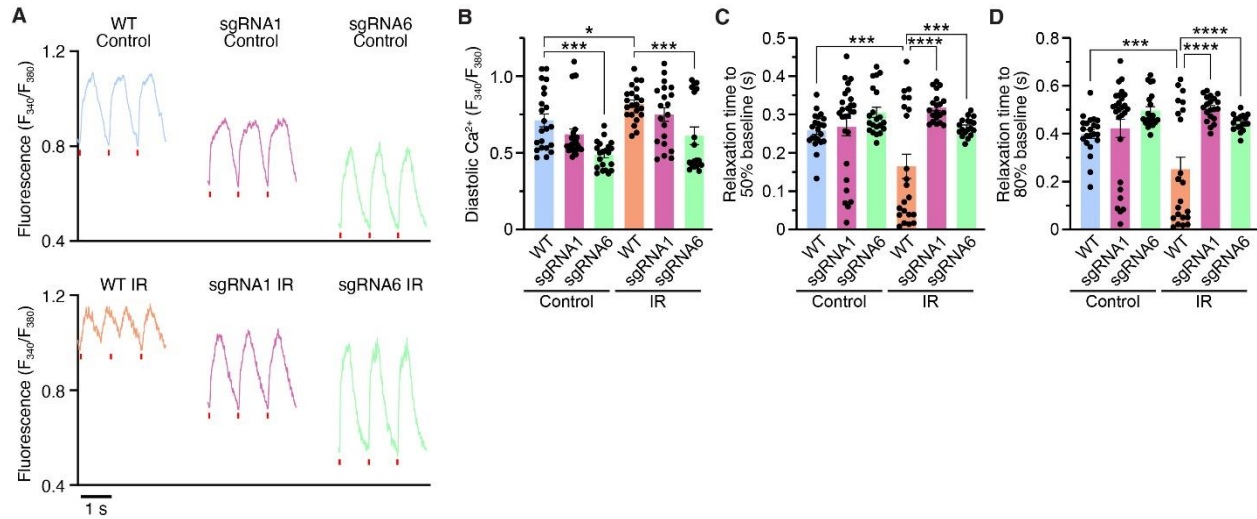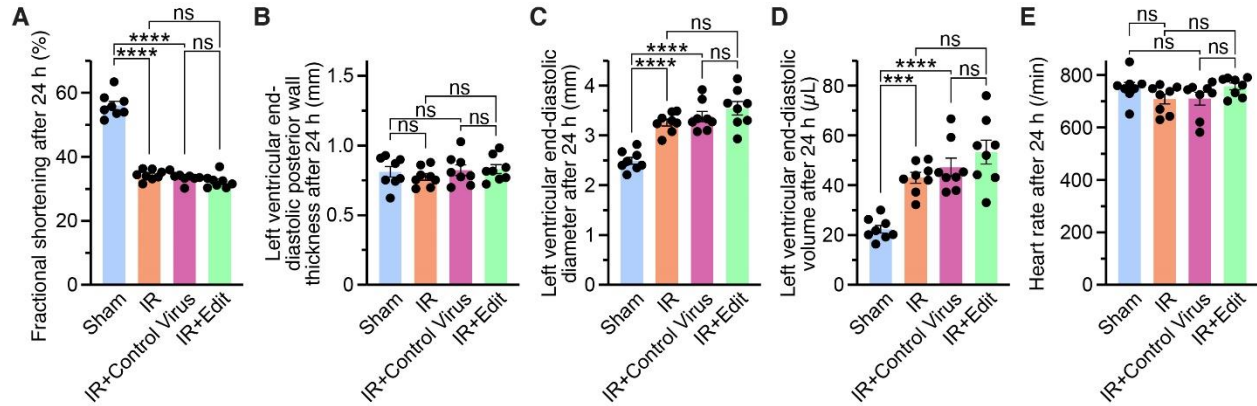
Fig. S4. *CaMKIIδ* **editing preserves cellular Ca²⁺ homeostasis in human iPSC-cardiomyocytes post-IR.** **(A)** Representative Ca²⁺ transients for human wildtype (WT), sgRNA1, and sgRNA6 iPSC-CMs for control group and following simulated ischemia/reperfusion (IR), as measured by epifluorescence microscopy. **(B)** Mean diastolic Ca²⁺ levels. **(C)** Mean relaxation time to 50% baseline. **(D)** Mean relaxation time to 80% baseline. Statistical comparisons are based on the number of cardiomyocytes and were performed with one-way ANOVA post-hoc corrected by Holm-Sidak. Data are presented as individual data points with means ± SEM.
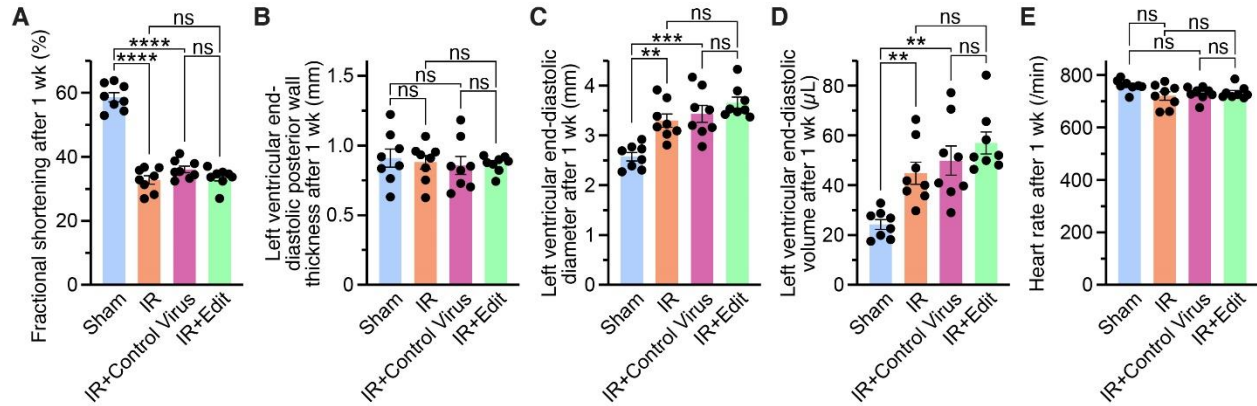
Fig. S5. Testing of mouse-sgRNA6 in mouse N2a cells. **(A)** Sequence of mouse *CaMKIIδ* gene encoding part of the regulatory domain and alignment of mouse-sgRNA6 (PAM sequence in green). Both ATGs encoding methionines are highlighted in yellow. Adenines along the sequence of sgRNA6 are numbered (starting from the PAM). Bases that are different from the human sequence are marked with an asterisk. Mouse-sgRNA6 sequence has 95% homology with the human-sgRNA6 sequence. **(B)** Percentage of adenine (A) to guanine (G) editing in mouse N2a cells for each adenine in sgRNA6 following base editing with ABE8e and mouse-sgRNA6, as determined by Sanger sequencing. **(C)** Representative Sanger sequencing chromatogram for editing the mouse genome with sgRNA6. Data are presented as individual data points with means.
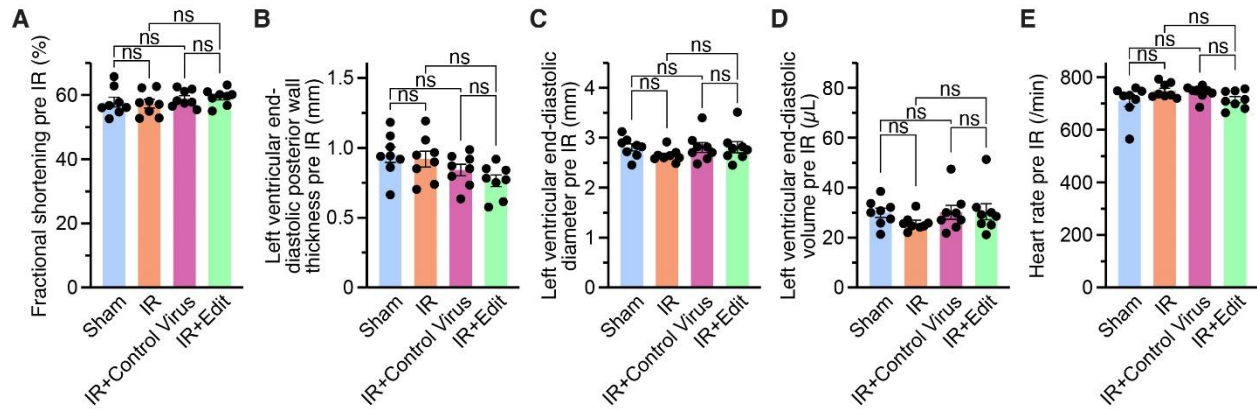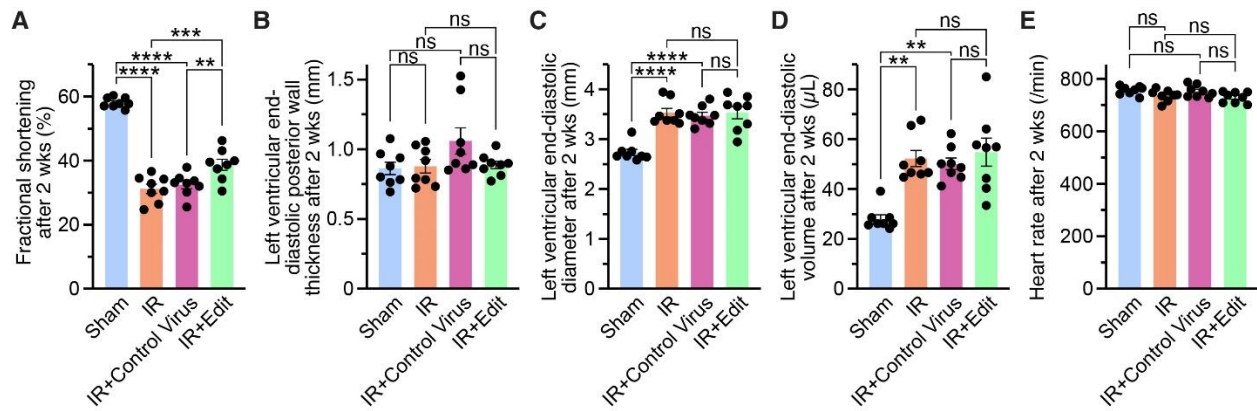
Fig. S6. Evaluation of cardiac function with echocardiography one week before ischemia/reperfusion injury. (A) Mean fractional shortening for sham-treated mice and mice subjected to ischemia/reperfusion (IR) injury with either no injection, injection of a control virus or intracardiac injection of AAV-ABE-sgRNA6 (IR+Edit). **(B)** Mean left ventricular end-diastolic posterior wall thickness for all groups. **(C)** Mean left ventricular end-diastolic diameter for all groups. **(D)** Mean left ventricular end-diastolic volume for all groups. **(E)** Mean heart rate for all groups. Statistical comparisons are based on eight mice per group and were performed with one-way ANOVA post-hoc corrected by Holm-Sidak. Data are presented as individual data points with means ± SEM.
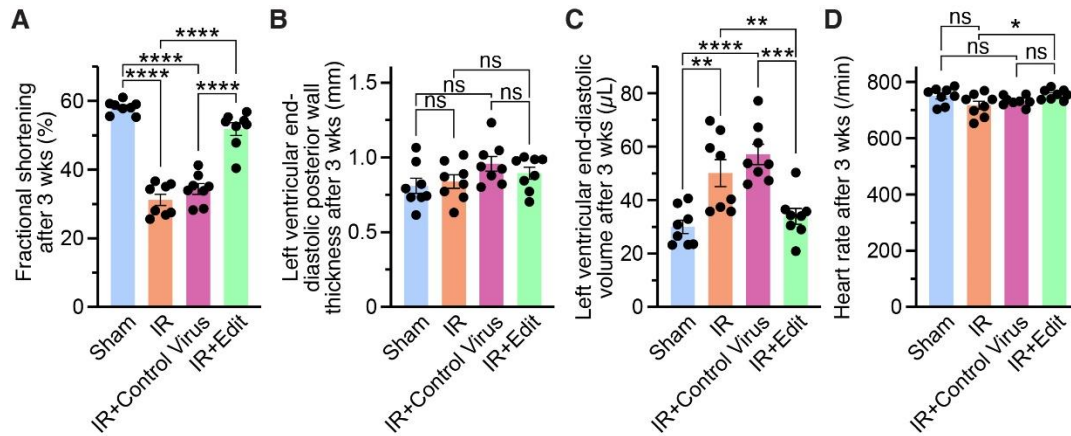
Fig. S7. Evaluation of cardiac function with echocardiography 24 hours after ischemia/reperfusion injury. (A) Mean fractional shortening for sham-treated mice and mice subjected to ischemia/reperfusion (IR) injury with either no injection, injection of a control virus or intracardiac injection of AAV-ABE-sgRNA6 (IR+Edit). **(B)** Mean left ventricular end-diastolic posterior wall thickness for all groups. **(C)** Mean left ventricular end-diastolic diameter for all groups. **(D)** Mean left ventricular end-diastolic volume for all groups. **(E)** Mean heart rate for all groups. Statistical comparisons are based on eight mice per group and were performed with one-way ANOVA post-hoc corrected by Holm-Sidak. Data are presented as individual data points with means ± SEM.
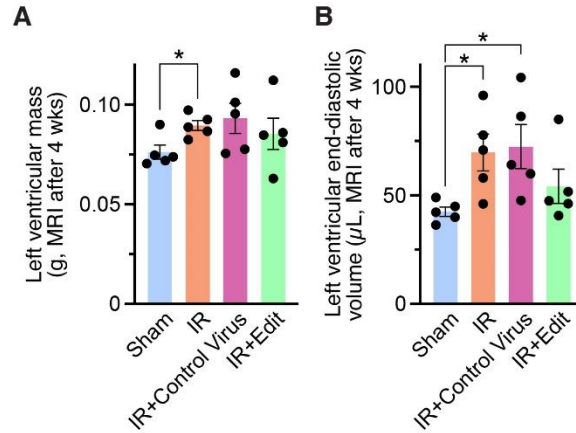
Fig. S8. Evaluation of cardiac function with echocardiography one week after ischemia/reperfusion injury. (A) Mean fractional shortening for sham-treated mice and mice subjected to ischemia/reperfusion (IR) injury with either no injection, injection of a control virus or intracardiac injection of AAV-ABE-sgRNA6 (IR+Edit). **(B)** Mean left ventricular end-diastolic posterior wall thickness for all groups. **(C)** Mean left ventricular end-diastolic diameter for all groups. **(D)** Mean left ventricular end-diastolic volume for all groups. **(E)** Mean heart rate for all groups. Statistical comparisons are based on eight mice per group and were performed with one-way ANOVA post-hoc corrected by Holm-Sidak. Data are presented as individual data points with means ± SEM.

Fig. S9. Evaluation of cardiac function with echocardiography two weeks after ischemia/reperfusion injury. (A) Mean fractional shortening for sham-treated mice and mice subjected to ischemia/reperfusion (IR) injury with either no injection, injection of a control virus or intracardiac injection of AAV-ABE-sgRNA6 (IR+Edit). **(B)** Mean left ventricular end-diastolic posterior wall thickness for all groups. **(C)** Mean left ventricular end-diastolic diameter for all groups. **(D)** Mean left ventricular end-diastolic volume for all groups. **(E)** Mean heart rate for all groups. Statistical comparisons are based on eight mice per group and were performed with one-way ANOVA post-hoc corrected by Holm-Sidak (A-C and E) and with Kruskal-Wallis test post-hoc corrected by Dunn (D). Data are presented as individual data points with means ± SEM.

Fig. S10. Evaluation of cardiac function with echocardiography three weeks after ischemia/reperfusion injury. (A) Mean fractional shortening for sham-treated mice and mice subjected to ischemia/reperfusion (IR) injury with either no injection, injection of a control virus or intracardiac injection of AAV-ABE-sgRNA6 (IR+Edit). **(B)** Mean left ventricular end-diastolic posterior wall thickness for all groups. **(C)** Mean left ventricular end-diastolic volume for all groups. **(D)** Mean heart rate for all groups. Statistical comparisons are based on eight mice per group and were performed with one-way ANOVA post-hoc corrected by Holm-Sidak. Data are presented as individual data points with means ± SEM.

Fig. S11. Evaluation of cardiac function with cardiac magnetic resonance imaging four weeks after ischemia/reperfusion injury. **(A)** Mean left ventricular mass for sham-treated mice and mice subjected to ischemia/reperfusion (IR) injury with either no injection, injection of a control virus or intracardiac injection of AAV-ABE-sgRNA6 (IR+Edit). **(B)** Mean left ventricular end-diastolic volume for all groups. Statistical comparisons are based on five mice per group and were performed with Kruskal-Wallis test post-hoc corrected by Dunn (A) and one-way ANOVA post-hoc corrected by Holm-Sidak (B). Data are presented as individual data points with means ± SEM.
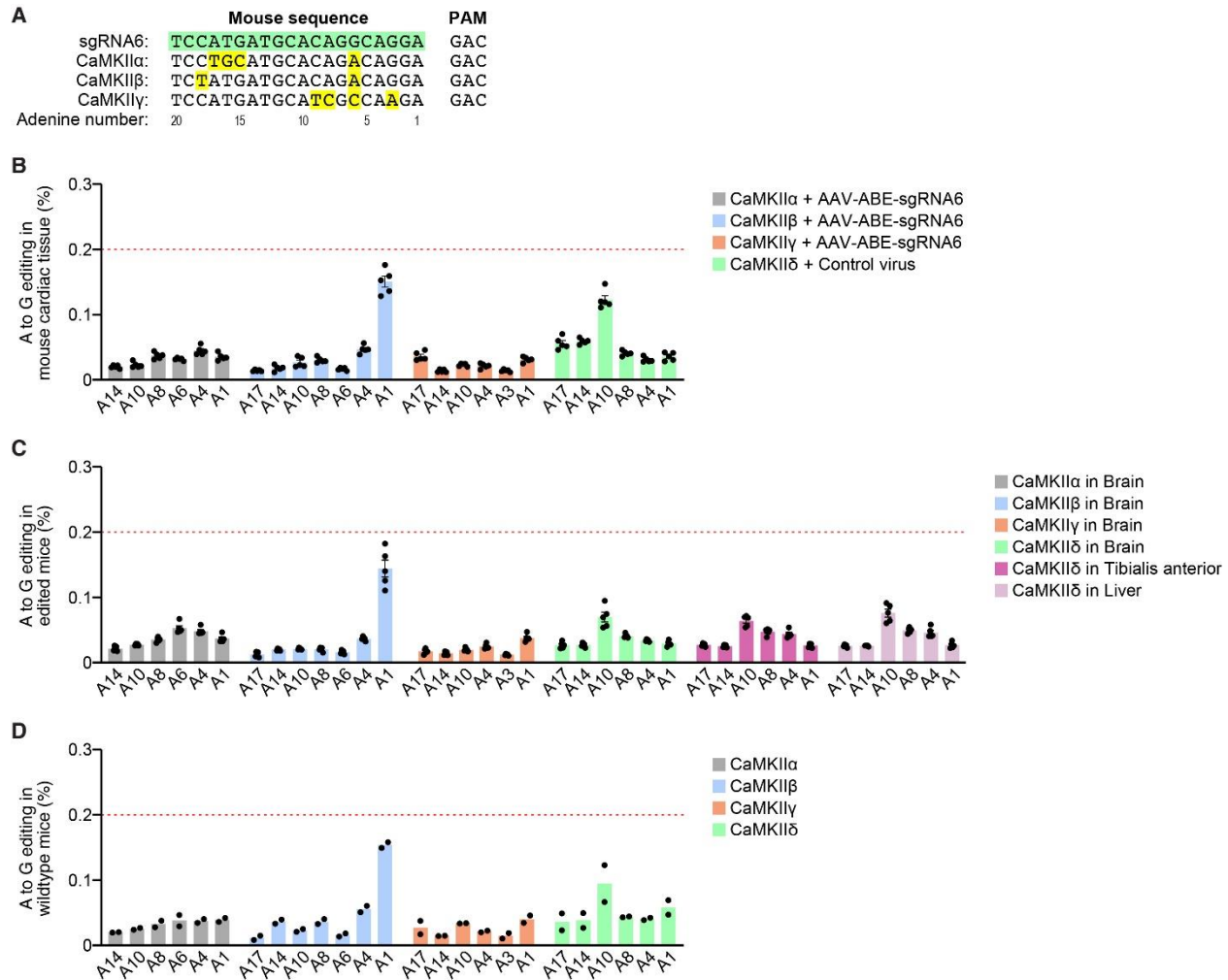
Fig. S12. Analysis of potential genomic off-targets in mouse tissue using deep amplicon sequencing. (**A**) Mouse sequence of sgRNA6 and the corresponding DNA sequences and PAMs of other *CaMKII* isoforms (α, β, and γ) in the mouse genome. Bases that are different from sgRNA6 are highlighted in yellow. Adenines along the sequence are numbered starting from the PAM. (**B**) Percentage of cardiac adenine (A) to guanine (G) editing for each adenine in the DNA sequence corresponding to sgRNA6 in different *CaMKII* isoforms. Mice were either injected with AAV-ABE-sgRNA6 (IR+Edit; for analyses of *CaMKIIα, β,* and *γ*) or with a control virus (for analysis of *CaMKIIδ*). (**C**) Percentage of A to G editing for each adenine in the DNA sequence corresponding to sgRNA6 in the brain (for all *CaMKII* isoforms), the tibialis anterior muscle (for *CaMKIIδ*), and the liver (for *CaMKIIδ*) of mice injected with AAV-ABE-sgRNA6 (IR+Edit). (**D**) Percentage of A to G editing for each adenine in the DNA sequence corresponding to sgRNA6 in all *CaMKII* isoforms, measured in wildtype control mice. The red line at 0.2% represents the threshold that has previously been used to distinguish from unspecific background guanine signal (*26*). Data are presented as individual data points with means ± SEM (B+C) or as individual data points with means (D).
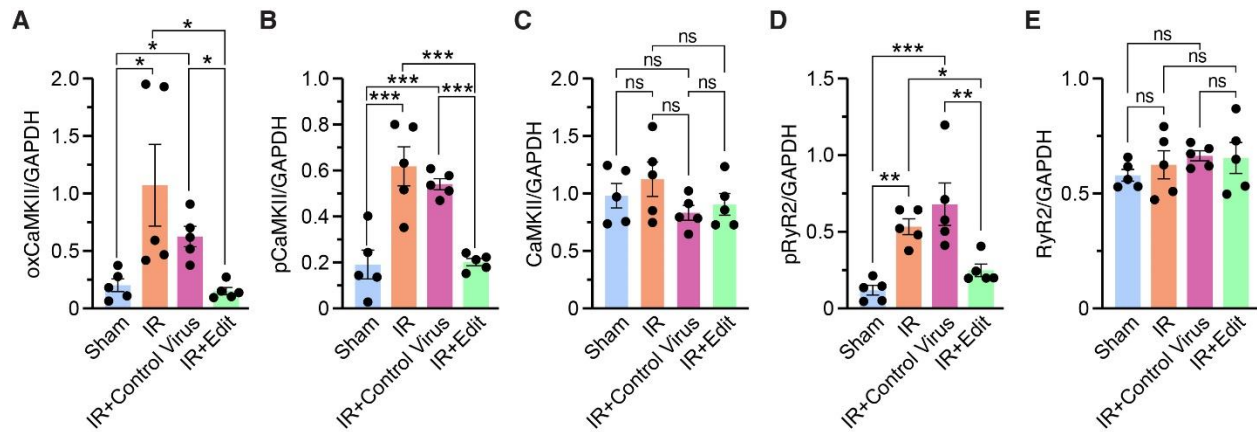
Fig. S13. Western blot analyses in mouse myocardium post-IR. (**A**) Mean densitometric analysis for oxidized CaMKII normalized to GAPDH for sham-treated mice and mice subjected to ischemia/reperfusion (IR) injury with either no injection, injection of a control virus or intracardiac injection of AAV-ABE-sgRNA6 (IR+Edit). (**B**) Mean densitometric analysis for autophosphorylated CaMKII normalized to GAPDH. (**C**) Mean densitometric analysis for total CaMKII normalized to GAPDH. (**D**) Mean densitometric analysis for ryanodine receptor type 2 (RyR2) phosphorylation at the CaMKII site (serine 2814) normalized to GAPDH. (**E**) Mean densitometric analysis for total RyR2 normalized to GAPDH. These data represent further densitometric analyses related to the Western blots presented in the main manuscript. Representative Western blots can be found in Fig. 3E (for A, B, and C) and Fig. 3I (for D and E). Statistical comparisons are based on five mice per group and were performed with one-way ANOVA post-hoc corrected by Holm-Sidak. Data are presented as individual data points with means ± SEM.
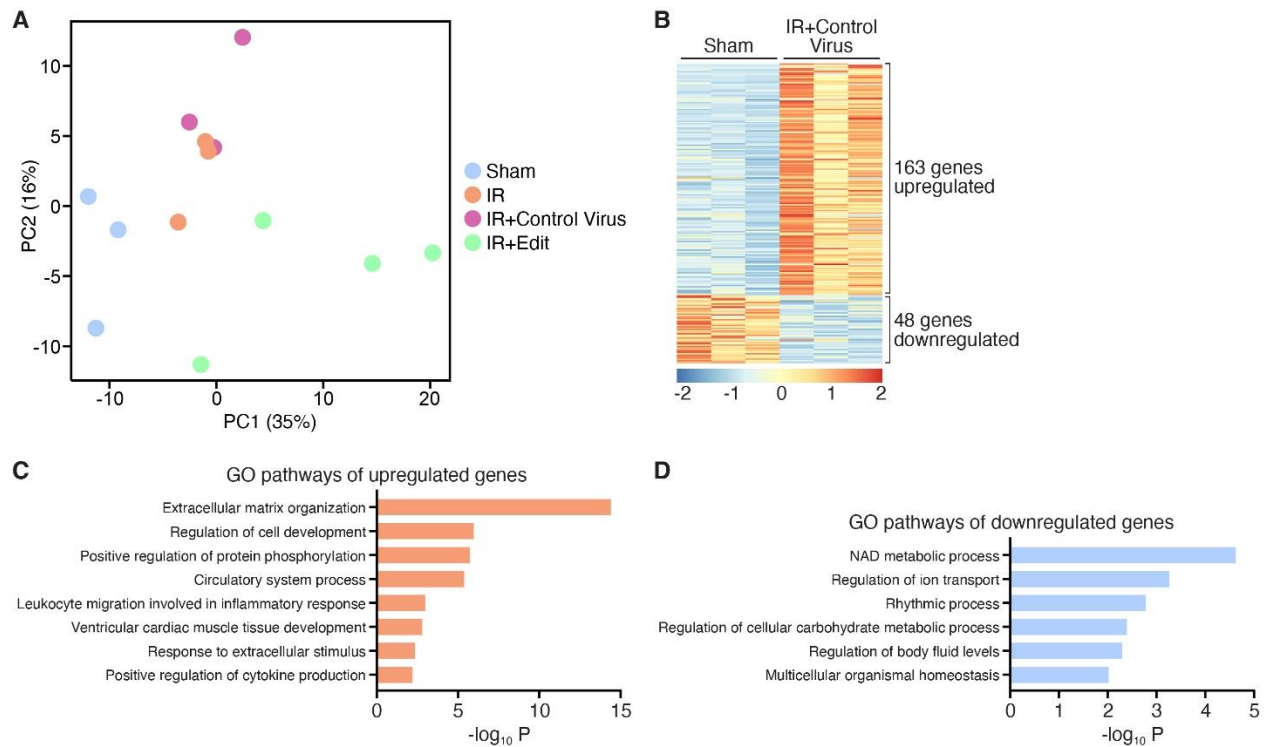
Fig. S14. Analysis of the cardiac transcriptome post-IR using RNA sequencing. (A) Principal component analysis (PCA) of the cardiac transcriptome of sham-treated mice (n=3) and mice subjected to ischemia/reperfusion (IR) injury with either no injection (n=3), injection of a control virus (n=3) or intracardiac injection of AAV-ABE-sgRNA6 (IR+Edit; n=4). **(B)** Heat map of the 211 differentially expressed genes between sham-treated mice and mice subjected to IR with injection of a control virus. **(C)** Gene ontology terms associated with the 163 genes upregulated in mice subjected to IR and a control virus. **(D)** Gene ontology terms associated with the 48 genes downregulated in mice subjected to IR and a control virus. Data are presented as individual data points.
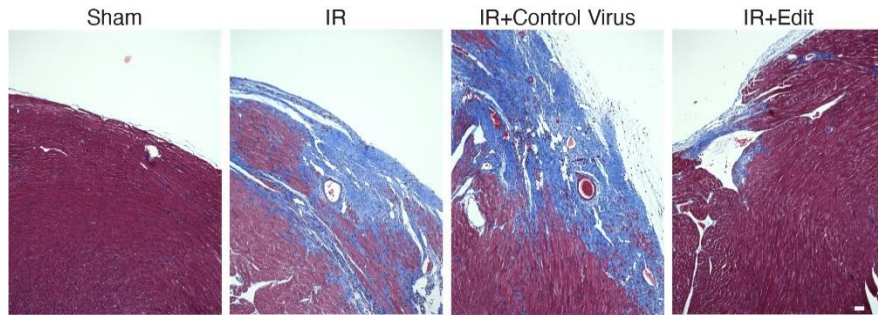
Fig. S15. Genomic editing of *CaMKIIδ* gene prevents myocardial fibrosis and infiltration of inflammatory cells post-IR. Transverse cross-sections of trichrome stained hearts for one sham-treated mouse and mice subjected to ischemia/reperfusion (IR) injury with either no injection, injection of a control virus or injection of AAV-ABE-sgRNA6 (IR+Edit; 10x magnification, scale bar 50 μm).
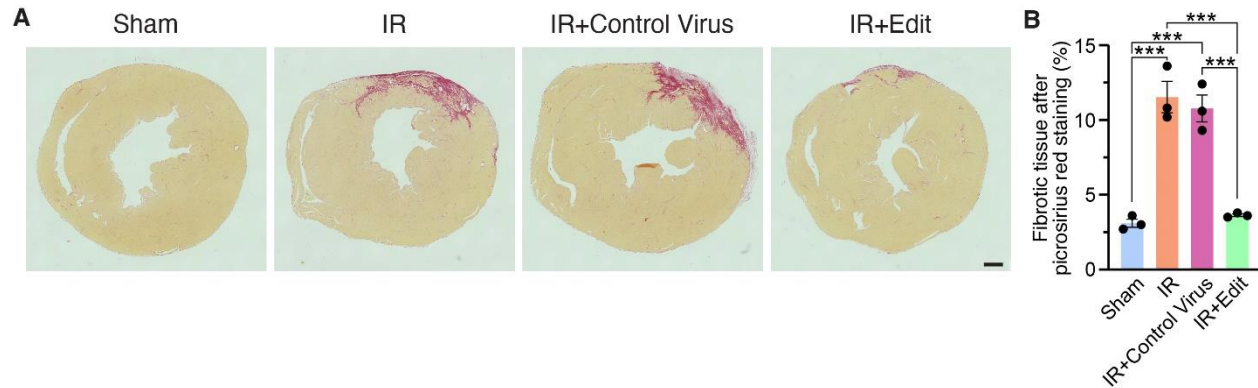
Fig. S16. Decreased fibrosis in *CaMKIIδ* edited mice post-IR. (A) Whole transverse cross-sections of picrosirius red stained hearts for one sham-treated mouse and mice subjected to ischemia/reperfusion (IR) injury with either no injection, injection of a control virus or injection of AAV-ABE-sgRNA6 (IR+Edit; scale bar 500 μm). **(B)** Mean percentage of fibrotic cardiac tissue in each group. Replicates are individual mice. Statistical comparisons are based on one-way ANOVA post-hoc corrected by Holm-Sidak. Data are presented as individual data points with means ± SEM.
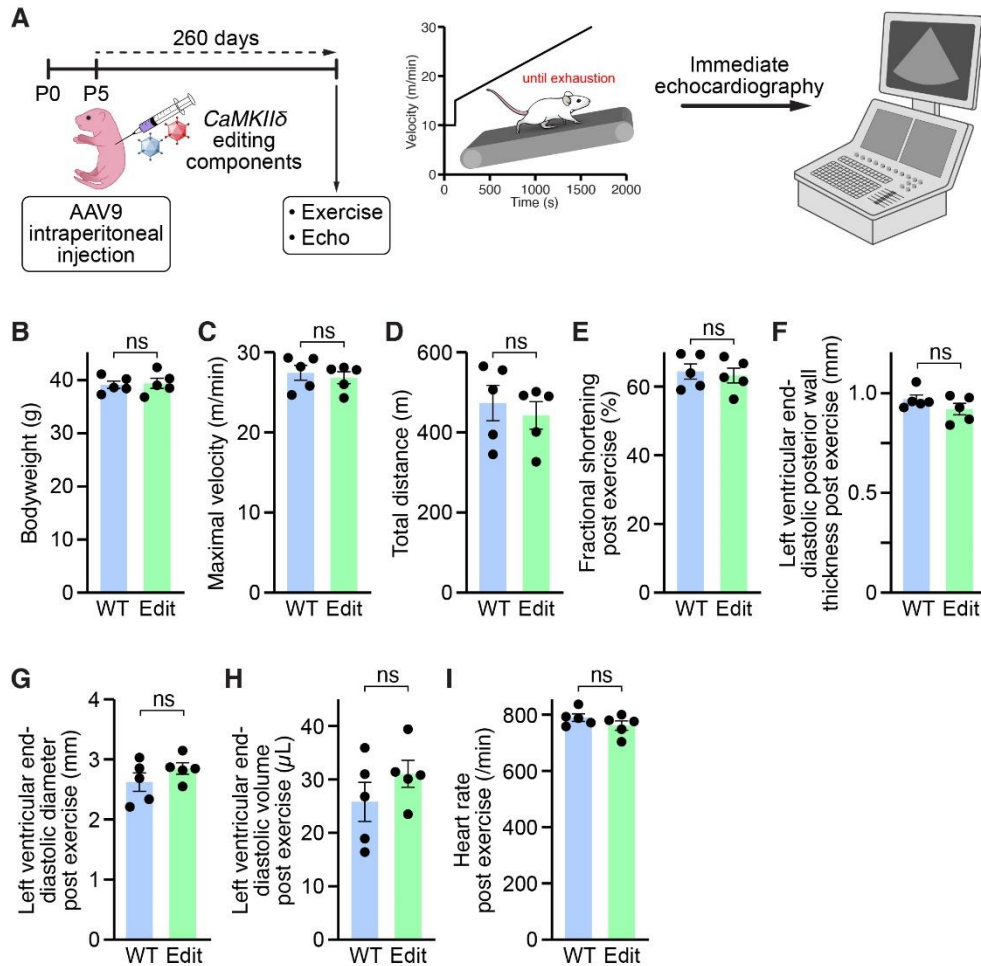
Fig. S17. Preserved exercise performance 260 days after systemic administration of AAV-ABE-sgRNA6. (**A**) Experimental design to investigate potential long-term adverse effects of *CaMKIIδ* gene editing. Mice were subjected to a treadmill exhaustion test 260 days after intraperitoneal administration of AAV-ABE-sgRNA6. After exhaustion, cardiac function was immediately assessed using echocardiography. (**B**) Mean bodyweight of *CaMKIIδ* edited mice (Edit) and their non-injected littermates (WT). (**C**) Mean maximal velocity achieved on the treadmill for both groups. (**D**) Mean distance attained on the treadmill prior to exhaustion for both groups. (**E**) Mean fractional shortening immediately after exhaustion. (**F**) Mean left ventricular end-diastolic posterior wall thickness. (**G**) Mean left ventricular end-diastolic diameter. (**H**) Mean left ventricular end-diastolic volume. (**I**) Mean heart rate. Replicates are five individual mice per group. Statistical comparisons are based on unpaired Student's *t* tests. Data are presented as individual data points with means ± SEM.

Supplementary Tables

Table S1. Sequences of sgRNAs tested in this study.

sgRNA	Sequence	PAM
Human-sgRNA1	TGCTTCCATGATGCACAGAC	AGG
Human-sgRNA2	GCTTCCATGATGCACAGACA	GG
Human-sgRNA3	TTCCATGATGCACAGACAGG	AG
Human-sgRNA4	ATGATGCACAGACAGGAGAC	TG
Human-sgRNA5	CTTCCATGATGCACAGACAG	GAG
Human-sgRNA6	TCCATGATGCACAGACAGGA	GAC
Mouse-sgRNA6	TCCATGATGCACAGGCAGGA	GAC

Table S2. Primers used for Sanger sequencing analyses.

Target	Primer	Sequence
Human *CaMKIIδ* DNA	Forward	GCTAAGGTGATAAATGTGGCACT
	Reverse	CTAGTGTGCGGGCCAGATTC
Mouse *CaMKIIδ* DNA	Forward	TGGCTGCAGTAGTGTGACTG
	Reverse	CAGGTAGCAAGGGCTCACAA

Table S3. Primers for deep amplicon sequencing of *CaMKIIα*, *β*, *γ* and *δ*.

On-target	Primer	Sequence
Human *CaMKIIα* DNA	Forward	TCGTCGGCAGCGTCAGATGTGTATAAGAGACAGCTTCCACTCACAGCCCTCTC
	Reverse	GTCTCGTGGGCTCGGAGATGTGTATAAGAGACAGGAGCAAGGGCTCAGTCATTC
Human *CaMKIIβ* DNA	Forward	TCGTCGGCAGCGTCAGATGTGTATAAGAGACAGGCCATATGACCACCCATTTC
	Reverse	GTCTCGTGGGCTCGGAGATGTGTATAAGAGACAGCAACTAGGAGGAGCCACACC
Human *CaMKIIγ* DNA	Forward	TCGTCGGCAGCGTCAGATGTGTATAAGAGACAGCCTTGAGTTTCGGGTAGTGC
	Reverse	GTCTCGTGGGCTCGGAGATGTGTATAAGAGACAGTCCTGGCTAGAGCCTGAAGA
Human *CaMKIIδ* DNA	Forward	TCGTCGGCAGCGTCAGATGTGTATAAGAGACAGCGTCAGTGTTGCATCTTGGT
	Reverse	GTCTCGTGGGCTCGGAGATGTGTATAAGAGACAGCCAAGAGCCCCAAAAAGAAT
Mouse *CaMKIIα* DNA	Forward	TCGTCGGCAGCGTCAGATGTGTATAAGAGACAGCTCCAGGTCTTGTTCCGTGT
	Reverse	GTCTCGTGGGCTCGGAGATGTGTATAAGAGACAGACATGCATGAAACCGATGAA
Mouse *CaMKIIβ* DNA	Forward	TCGTCGGCAGCGTCAGATGTGTATAAGAGACAGGATGATCCTCACTGCCCTGT
	Reverse	GTCTCGTGGGCTCGGAGATGTGTATAAGAGACAGGAAGCGACCAGCTCTGTACC
Mouse *CaMKIIγ* DNA	Forward	TCGTCGGCAGCGTCAGATGTGTATAAGAGACAGCCTATCCTGGCTCAGTGCTC
	Reverse	GTCTCGTGGGCTCGGAGATGTGTATAAGAGACAGAGTCCCGTGAGTTCAGATGG
Mouse *CaMKIIδ* DNA	Forward	TCGTCGGCAGCGTCAGATGTGTATAAGAGACAGGCCCTAAGGAAAAACCAAGG
	Reverse	GTCTCGTGGGCTCGGAGATGTGTATAAGAGACAGCCTCCCACAACAATGTCAAA
Mouse CaMKIIδ cDNA	Forward	TCGTCGGCAGCGTCAGATGTGTATAAGAGACAGCTGGCACACCTGGGTATCTT
	Reverse	GTCTCGTGGGCTCGGAGATGTGTATAAGAGACAGTCGTAGCCAGCATAGTTGTCA

Table S4. Analysis of potential off-target editing sites in the human genome, as predicted by CRISPOR.

#	Gene	Locus	Sequence	PAM	CFD-Score
1	Intron *RP11-707M1.1*	Chr11_49743055	ACCATAATGCACAAACATGA	AGG	0.5
2	Intron *GRM5*	Chr11_88634755	ACCATAATGCACAAACATGA	AGG	0.5
3	Intergenic *URGCP/URGCP-MRPS24|URGCP*	Chr7_43937791	TCCATAATGCAAAGAAATGA	TGG	0.47
4	Intergenic *snoU13|TOX*	Chr8_59615439	GTCATGATGCACAAACAGAA	GGG	0.46
5	Intergenic *FTH1P22|AL157904.1*	Chr1_117361285	TTAATGATGCAAAGACAGAA	GGG	0.4
6	Intergenic *snoZ247|LDHAP3*	Chr2_41988088	ACCATGAACAACAGACAGGA	GGG	0.37
7	Intergenic *FAM155A|SNORD31*	Chr13_107879509	TGCATGATGCACAAACAGAA	TGG	0.37
8	Intron *DAZL*	Chr3_16638794	TTCATGAACTACAGACAGGA	AGG	0.36

Table S5. Primers for deep amplicon sequencing of potential off-target editing sites in the human genome.

Off-target	Primer	Sequence
1	Forward	TCGTCGGCAGCGTCAGATGTGTATAAGAGACAGATTCAGAATAGGCGGCTTCA
	Reverse	GTCTCGTGGGCTCGGAGATGTGTATAAGAGACAGGTCGTTTCCAGCCTTCATGT
2	Forward	TCGTCGGCAGCGTCAGATGTGTATAAGAGACAGGTGATGGCAACACAGCAGAG
	Reverse	GTCTCGTGGGCTCGGAGATGTGTATAAGAGACAGTGGAAAAACCTCGCTCAACT
3	Forward	TCGTCGGCAGCGTCAGATGTGTATAAGAGACAGGGAGGTCTGTGGGTAAAGCA
	Reverse	GTCTCGTGGGCTCGGAGATGTGTATAAGAGACAGGTATGTCCCCGGCTTACTGA
4	Forward	TCGTCGGCAGCGTCAGATGTGTATAAGAGACAGACCATTGCCATTCACCTCAT
	Reverse	GTCTCGTGGGCTCGGAGATGTGTATAAGAGACAGGGCCTGCTTCCTGATTCATA
5	Forward	TCGTCGGCAGCGTCAGATGTGTATAAGAGACAGACTTCAAAGTGGGGCAAGTG
	Reverse	GTCTCGTGGGCTCGGAGATGTGTATAAGAGACAGTGCAGCATTTGGAAACCATA
6	Forward	TCGTCGGCAGCGTCAGATGTGTATAAGAGACAGGAAGGGGAACCAAAGGAAAG
	Reverse	GTCTCGTGGGCTCGGAGATGTGTATAAGAGACAGTGCAGGTACTCTGGCAGTTG
7	Forward	TCGTCGGCAGCGTCAGATGTGTATAAGAGACAGGCCAGAGTTCATCTCCCAGA
	Reverse	GTCTCGTGGGCTCGGAGATGTGTATAAGAGACAGATGCGGGTATCATGAAATGG
8	Forward	TCGTCGGCAGCGTCAGATGTGTATAAGAGACAGAATCAGTGTCAAGAGGCATCAA
	Reverse	GTCTCGTGGGCTCGGAGATGTGTATAAGAGACAGAATGACGTGGATGTGCAGAA

Captions for Supplementary Movies

Movie S1. MRI cine data in four-chamber view for one representative sham-treated mouse.

Movie S2. MRI cine data in four-chamber view for one representative mouse subjected to IR.

Movie S3. MRI cine data in four-chamber view for one representative mouse subjected to IR with intracardiac injection of a control virus.

Movie S4. MRI cine data in four-chamber view for one representative mouse subjected to IR with intracardiac injection of AAV-ABE-sgRNA6 (IR+Edit).

References and Notes

1. N. Liu, E. N. Olson, CRISPR Modeling and Correction of Cardiovascular Disease. *Circ. Res.* **130**, 1827–1850 (2022). doi:10.1161/CIRCRESAHA.122.320496 Medline

2. F. Chemello, A. C. Chai, H. Li, C. Rodriguez-Caycedo, E. Sanchez-Ortiz, A. Atmanli, A. A. Mireault, N. Liu, R. Bassel-Duby, E. N. Olson, Precise correction of Duchenne muscular dystrophy exon deletion mutations by base and prime editing. *Sci. Adv.* **7**, eabg4910 (2021). doi:10.1126/sciadv.abg4910 Medline

3. M. F. Richter, K. T. Zhao, E. Eton, A. Lapinaite, G. A. Newby, B. W. Thuronyi, C. Wilson, L. W. Koblan, J. Zeng, D. E. Bauer, J. A. Doudna, D. R. Liu, Phage-assisted evolution of an adenine base editor with improved Cas domain compatibility and activity. *Nat. Biotechnol.* **38**, 883–891 (2020). [doi:10.1038/s41587-020-0453-z](doi:10.1038/s41587-020-0453-z) Medline

4. L. Amoasii, J. C. W. Hildyard, H. Li, E. Sanchez-Ortiz, A. Mireault, D. Caballero, R. Harron, T.-R. Stathopoulou, C. Massey, J. M. Shelton, R. Bassel-Duby, R. J. Piercy, E. N. Olson, Gene editing restores dystrophin expression in a canine model of Duchenne muscular dystrophy. *Science* **362**, 86–91 (2018). doi:10.1126/science.aau1549 Medline

5. L. Amoasii, H. Li, Y. Zhang, Y.-L. Min, E. Sanchez-Ortiz, J. M. Shelton, C. Long, A. A. Mireault, S. Bhattacharyya, J. R. McAnally, R. Bassel-Duby, E. N. Olson, In vivo non-invasive monitoring of dystrophin correction in a new Duchenne muscular dystrophy reporter mouse. *Nat. Commun.* **10**, 4537 (2019). [doi:10.1038/s41467-019-12335-x](doi:10.1038/s41467-019-12335-x) Medline

6. L. W. Koblan, M. R. Erdos, C. Wilson, W. A. Cabral, J. M. Levy, Z.-M. Xiong, U. L. Tavarez, L. M. Davison, Y. G. Gete, X. Mao, G. A. Newby, S. P. Doherty, N. Narisu, Q. Sheng, C. Krilow, C. Y. Lin, L. B. Gordon, K. Cao, F. S. Collins, J. D. Brown, D. R. Liu, In vivo base editing rescues Hutchinson-Gilford progeria syndrome in mice. *Nature* **589**, 608–614 (2021). [doi:10.1038/s41586-020-03086-7](doi:10.1038/s41586-020-03086-7) Medline

7. S. S. Virani, A. Alonso, H. J. Aparicio, E. J. Benjamin, M. S. Bittencourt, C. W. Callaway, A. P. Carson, A. M. Chamberlain, S. Cheng, F. N. Delling, M. S. V. Elkind, K. R. Evenson, J. F. Ferguson, D. K. Gupta, S. S. Khan, B. M. Kissela, K. L. Knutson, C. D. Lee, T. T. Lewis, J. Liu, M. S. Loop, P. L. Lutsey, J. Ma, J. Mackey, S. S. Martin, D. B. Matchar, M. E. Mussolino, S. D. Navaneethan, A. M. Perak, G. A. Roth, Z. Samad, G. M. Satou, E. B. Schroeder, S. H. Shah, C. M. Shay, A. Stokes, L. B. VanWagner, N.-Y. Wang, C. W. Tsao; American Heart Association Council on Epidemiology and Prevention Statistics Committee and Stroke Statistics Subcommittee, Heart Disease and Stroke Statistics–2021 Update *Circulation* **143**, e254–e743 (2021). [doi:10.1161/CIR.0000000000000950](doi:10.1161/CIR.0000000000000950) Medline

8. J. Beckendorf, M. M. G. van den Hoogenhof, J. Backs, Physiological and unappreciated roles of CaMKII in the heart. *Basic Res. Cardiol.* **113**, 29 (2018). [doi:10.1007/s00395-018-0688-8](doi:10.1007/s00395-018-0688-8) Medline

9. S. Neef, N. Dybkova, S. Sossalla, K. R. Ort, N. Fluschnik, K. Neumann, R. Seipelt, F. A. Schöndube, G. Hasenfuss, L. S. Maier, CaMKII-dependent diastolic SR Ca2+ leak and elevated diastolic Ca2+ levels in right atrial myocardium of patients with atrial fibrillation. *Circ. Res.* **106**, 1134–1144 (2010). doi:10.1161/CIRCRESAHA.109.203836 Medline

10. J. Backs, T. Backs, S. Neef, M. M. Kreusser, L. H. Lehmann, D. M. Patrick, C. E. Grueter, X. Qi, J. A. Richardson, J. A. Hill, H. A. Katus, R. Bassel-Duby, L. S. Maier, E. N. Olson, The delta isoform of CaM kinase II is required for pathological cardiac hypertrophy and remodeling after pressure overload. *Proc. Natl. Acad. Sci. U.S.A.* **106**, 2342–2347 (2009). doi:10.1073/pnas.0813013106 Medline

11. S. Lebek, K. Pichler, K. Reuthner, M. Trum, M. Tafelmeier, J. Mustroph, D. Camboni, L. Rupprecht, C. Schmid, L. S. Maier, M. Arzt, S. Wagner, Enhanced CaMKII-Dependent Late I_{Na} Induces Atrial Proarrhythmic Activity in Patients With Sleep-Disordered Breathing. *Circ. Res.* **126**, 603–615 (2020). doi:10.1161/CIRCRESAHA.119.315755 Medline

12. T. Zhang, J. H. Brown, Role of Ca2+/calmodulin-dependent protein kinase II in cardiac hypertrophy and heart failure. *Cardiovasc. Res.* **63**, 476–486 (2004). doi:10.1016/j.cardiores.2004.04.026 Medline

13. H. Ling, C. B. B. Gray, A. C. Zambon, M. Grimm, Y. Gu, N. Dalton, N. H. Purcell, K. Peterson, J. H. Brown, Ca2+/Calmodulin-dependent protein kinase II δ mediates myocardial ischemia/reperfusion injury through nuclear factor-κB. *Circ. Res.* **112**, 935–944 (2013). doi:10.1161/CIRCRESAHA.112.276915 Medline

14. M. Luo, X. Guan, E. D. Luczak, D. Lang, W. Kutschke, Z. Gao, J. Yang, P. Glynn, S. Sossalla, P. D. Swaminathan, R. M. Weiss, B. Yang, A. G. Rokita, L. S. Maier, I. R. Efimov, T. J. Hund, M. E. Anderson, Diabetes increases mortality after myocardial infarction by oxidizing CaMKII. *J. Clin. Invest.* **123**, 1262–1274 (2013). [doi:10.1172/JCI65268](doi:10.1172/JCI65268) Medline

15. D. Nassal, D. Gratz, T. J. Hund, Challenges and Opportunities for Therapeutic Targeting of Calmodulin Kinase II in Heart. *Front. Pharmacol.* **11**, 35 (2020). doi:10.3389/fphar.2020.00035 Medline

16. P. Pellicena, H. Schulman, CaMKII inhibitors: From research tools to therapeutic agents. *Front. Pharmacol.* **5**, 21 (2014). doi:10.3389/fphar.2014.00021 Medline

17. S. Lebek, A. Plößl, M. Baier, J. Mustroph, D. Tarnowski, C. M. Lücht, S. Schopka, B. Flörchinger, C. Schmid, Y. Zausig, N. Pagratis, B. Marchand, D. O. Koltun, W. K. Hung, S. Ahmadyar, L. Belardinelli, L. S. Maier, S. Wagner, The novel CaMKII inhibitor GS-680 reduces diastolic SR Ca leak and prevents CaMKII-dependent pro-arrhythmic activity. *J. Mol. Cell. Cardiol.* **118**, 159–168 (2018). doi:10.1016/j.yjmcc.2018.03.020 Medline

18. J. R. Erickson, M. L. Joiner, X. Guan, W. Kutschke, J. Yang, C. V. Oddis, R. K. Bartlett, J. S. Lowe, S. E. O'Donnell, N. Aykin-Burns, M. C. Zimmerman, K. Zimmerman, A.-J. L. Ham, R. M. Weiss, D. R. Spitz, M. A. Shea, R. J. Colbran, P. J. Mohler, M. E. Anderson, A dynamic pathway for calcium-independent activation of CaMKII by methionine oxidation. *Cell* **133**, 462–474 (2008). doi:10.1016/j.cell.2008.02.048 Medline

19. A. Purohit, A. G. Rokita, X. Guan, B. Chen, O. M. Koval, N. Voigt, S. Neef, T. Sowa, Z. Gao, E. D. Luczak, H. Stefansdottir, A. C. Behunin, N. Li, R. N. El-Accaoui, B. Yang, P. D. Swaminathan, R. M. Weiss, X. H. T. Wehrens, L.-S. Song, D. Dobrev, L. S. Maier, M. E. Anderson, Oxidized Ca(2+)/calmodulin-dependent protein kinase II triggers atrial fibrillation. *Circulation* **128**, 1748–1757 (2013). doi:10.1161/CIRCULATIONAHA.113.003313 Medline

20. M. Zhang, H. Gao, D. Liu, X. Zhong, X. Shi, P. Yu, L. Jin, Y. Liu, Y. Tang, Y. Song, J. Liu, X. Hu, C.-Y. Li, L. Song, J. Qin, F. Wu, F. Lan, Y. Zhang, R.-P. Xiao, CaMKII-δ9 promotes cardiomyopathy through disrupting UBE2T-dependent DNA repair. *Nat. Cell Biol.* **21**, 1152–1163 (2019). [doi:10.1038/s41556-019-0380-8](doi:10.1038/s41556-019-0380-8) Medline

21. N. M. Gaudelli, A. C. Komor, H. A. Rees, M. S. Packer, A. H. Badran, D. I. Bryson, D. R. Liu, Programmable base editing of A•T to G•C in genomic DNA without DNA cleavage. *Nature* **551**, 464–471 (2017). doi:10.1038/nature24644 Medline

22. A. C. Komor, Y. B. Kim, M. S. Packer, J. A. Zuris, D. R. Liu, Programmable editing of a target base in genomic DNA without double-stranded DNA cleavage. *Nature* **533**, 420–424 (2016). doi:10.1038/nature17946 Medline

23. L. W. Koblan, J. L. Doman, C. Wilson, J. M. Levy, T. Tay, G. A. Newby, J. P. Maianti, A. Raguram, D. R. Liu, Improving cytidine and adenine base editors by expression optimization and ancestral reconstruction. *Nat. Biotechnol.* **36**, 843–846 (2018). [doi:10.1038/nbt.4172](doi:10.1038/nbt.4172) Medline

24. R. T. Walton, K. A. Christie, M. N. Whittaker, B. P. Kleinstiver, Unconstrained genome targeting with near-PAMless engineered CRISPR-Cas9 variants. *Science* **368**, 290–296 (2020). doi:10.1126/science.aba8853 Medline

25. J. P. Concordet, M. Haeussler, CRISPOR: Intuitive guide selection for CRISPR/Cas9 genome editing experiments and screens. *Nucleic Acids Res.* **46** (W1), W242–W245 (2018). [doi:10.1093/nar/gky354](doi:10.1093/nar/gky354) Medline

26. K. Clement, H. Rees, M. C. Canver, J. M. Gehrke, R. Farouni, J. Y. Hsu, M. A. Cole, D. R. Liu, J. K. Joung, D. E. Bauer, L. Pinello, CRISPResso2 provides accurate and rapid genome editing sequence analysis. *Nat. Biotechnol.* **37**, 224–226 (2019). [doi:10.1038/s41587-019-0032-3](doi:10.1038/s41587-019-0032-3) Medline

27. M. Uhlén, L. Fagerberg, B. M. Hallström, C. Lindskog, P. Oksvold, A. Mardinoglu, Å. Sivertsson, C. Kampf, E. Sjöstedt, A. Asplund, I. Olsson, K. Edlund, E. Lundberg, S. Navani, C. A.-K. Szigyarto, J. Odeberg, D. Djureinovic, J. O. Takanen, S. Hober, T. Alm, P.-H. Edqvist, H. Berling, H. Tegel, J. Mulder, J. Rockberg, P. Nilsson, J. M. Schwenk, M. Hamsten, K. von Feilitzen, M. Forsberg, L. Persson, F. Johansson, M. Zwahlen, G. von Heijne, J. Nielsen, F. Pontén, Tissue-based map of the human proteome. *Science* **347**, 1260419 (2015). doi:10.1126/science.1260419 Medline

28. Q. Wang, E. O. Hernández-Ochoa, M. C. Viswanathan, I. D. Blum, D. C. Do, J. M. Granger, K. R. Murphy, A.-C. Wei, S. Aja, N. Liu, C. M. Antonescu, L. D. Florea, C. C. Talbot Jr., D. Mohr, K. R. Wagner, S. Regot, R. M. Lovering, P. Gao, M. A. Bianchet, M. N. Wu, A. Cammarato, M. F. Schneider, G. S. Bever, M. E. Anderson, CaMKII oxidation is a critical performance/disease trade-off acquired at the dawn of vertebrate evolution. *Nat. Commun.* **12**, 3175 (2021). [doi:10.1038/s41467-021-23549-3](doi:10.1038/s41467-021-23549-3) Medline

29. B. Hegyi, Y. Chen-Izu, Z. Jian, R. Shimkunas, L. T. Izu, T. Banyasz, KN-93 inhibits IKr in mammalian cardiomyocytes. *J. Mol. Cell. Cardiol.* **89** (Pt B), 173–176 (2015). doi:10.1016/j.yjmcc.2015.10.012 Medline

30. D. R. Karri, Y. Zhang, F. Chemello, Y.-L. Min, J. Huang, J. Kim, P. P. A. Mammen, L. Xu, N. Liu, R. Bassel-Duby, E. N. Olson, Long-term maintenance of dystrophin expression

and resistance to injury of skeletal muscle in gene edited DMD mice. *Mol. Ther. Nucleic Acids* **28**, 154–167 (2022). doi:10.1016/j.omtn.2022.03.004 Medline

31. J. S. Lawton, J. E. Tamis-Holland, S. Bangalore, E. R. Bates, T. M. Beckie, J. M. Bischoff, J. A. Bittl, M. G. Cohen, J. M. DiMaio, C. W. Don, S. E. Fremes, M. F. Gaudino, Z. D. Goldberger, M. C. Grant, J. B. Jaswal, P. A. Kurlansky, R. Mehran, T. S. Metkus Jr., L. C. Nnacheta, S. V. Rao, F. W. Sellke, G. Sharma, C. M. Yong, B. A. Zwischenberger, 2021 ACC/AHA/SCAI Guideline for Coronary Artery Revascularization: A Report of the American College of Cardiology/American Heart Association Joint Committee on Clinical Practice Guidelines. *Circulation* **145**, e18–e114 (2022). doi:10.1161/CIR.0000000000001038 Medline

32. K. Musunuru, A. C. Chadwick, T. Mizoguchi, S. P. Garcia, J. E. DeNizio, C. W. Reiss, K. Wang, S. Iyer, C. Dutta, V. Clendaniel, M. Amaonye, A. Beach, K. Berth, S. Biswas, M. C. Braun, H.-M. Chen, T. V. Colace, J. D. Ganey, S. A. Gangopadhyay, R. Garrity, L. N. Kasiewicz, J. Lavoie, J. A. Madsen, Y. Matsumoto, A. M. Mazzola, Y. S. Nasrullah, J. Nneji, H. Ren, A. Sanjeev, M. Shay, M. R. Stahley, S. H. Y. Fan, Y. K. Tam, N. M. Gaudelli, G. Ciaramella, L. E. Stolz, P. Malyala, C. J. Cheng, K. G. Rajeev, E. Rohde, A. M. Bellinger, S. Kathiresan, In vivo CRISPR base editing of PCSK9 durably lowers cholesterol in primates. *Nature* **593**, 429–434 (2021). doi:10.1038/s41586-021-03534-y Medline

33. T. P. Huang, K. T. Zhao, S. M. Miller, N. M. Gaudelli, B. L. Oakes, C. Fellmann, D. F. Savage, D. R. Liu, Circularly permuted and PAM-modified Cas9 variants broaden the targeting scope of base editors. *Nat. Biotechnol.* **37**, 626–631 (2019). doi:10.1038/s41587-019-0134-y Medline

34. J. M. Levy, W.-H. Yeh, N. Pendse, J. R. Davis, E. Hennessey, R. Butcher, L. W. Koblan, J. Comander, Q. Liu, D. R. Liu, Cytosine and adenine base editing of the brain, liver, retina, heart and skeletal muscle of mice via adeno-associated viruses. *Nat. Biomed. Eng.* **4**, 97–110 (2020). doi:10.1038/s41551-019-0501-5 Medline

35. M. G. Kluesner, D. A. Nedveck, W. S. Lahr, J. R. Garbe, J. E. Abrahante, B. R. Webber, B. S. Moriarity, EditR: A Method to Quantify Base Editing from Sanger Sequencing. *CRISPR J* **1**, 239–250 (2018). doi:10.1089/crispr.2018.0014 Medline

36. G. Zhang, X. Wang, C. Li, Q. Li, Y. A. An, X. Luo, Y. Deng, T. G. Gillette, P. E. Scherer, Z. V. Wang, Integrated Stress Response Couples Mitochondrial Protein Translation With Oxidative Stress Control. *Circulation* **144**, 1500–1515 (2021). doi:10.1161/CIRCULATIONAHA.120.053125 Medline

37. E. Heiberg, J. Sjögren, M. Ugander, M. Carlsson, H. Engblom, H. Arheden, Design and validation of Segment—Freely available software for cardiovascular image analysis. *BMC Med. Imaging* **10**, 1 (2010). doi:10.1186/1471-2342-10-1 Medline

38. Y. Zhou, B. Zhou, L. Pache, M. Chang, A. H. Khodabakhshi, O. Tanaseichuk, C. Benner, S. K. Chanda, Metascape provides a biologist-oriented resource for the analysis of systems-level datasets. *Nat. Commun.* **10**, 1523 (2019). doi:10.1038/s41467-019-09234-6 Medline